HHS Public Access

Author manuscript

Nat Neurosci. Author manuscript; available in PMC 2018 May 06.

Published in final edited form as:

Nat Neurosci. 2017 December ; 20(12): 1761–1769. doi:10.1038/s41593-017-0007-y.

Weak correlations between hemodynamic signals and ongoing neural activity during the resting state

Aaron T. Winder[1,2], **Christina Echagarruga**[1,3], **Qingguang Zhang**[1,2], and **Patrick J. Drew**[1,2,3,4]

[1]Center for Neural Engineering, Pennsylvania State University, University Park, PA 16802

[2]Department of Engineering Science and Mechanics, Pennsylvania State University, University Park, PA 16802

[3]Graduate Program in Bioengineering, Pennsylvania State University, University Park, PA 16802

[4]Department of Neurosurgery and Department of Biomedical Engineering, Pennsylvania State University, University Park, PA 16802

Abstract

Spontaneous fluctuations in hemodynamic signals in the absence of a task or overt stimulation are used to infer neural activity. We tested this coupling by simultaneously measuring neural activity and changes in cerebral blood volume (CBV) in the somatosensory cortex of awake, head-fixed mice during periods of true rest, and during whisker stimulation and volitional whisking. Here we show that neurovascular coupling was similar across states, and large spontaneous CBV changes in the absence of sensory input were driven by volitional whisker and body movements. Hemodynamic signals during periods of rest were weakly correlated with neural activity. Spontaneous fluctuations in CBV and vessel diameter persisted when local neural spiking and glutamatergic input was blocked, and during blockade of noradrenergic receptors, suggesting a non-neuronal origin for spontaneous CBV fluctuations. Spontaneous hemodynamic signals reflect a combination of behavior, local neural activity, and putatively non-neural processes.

Introduction

Spontaneous hemodynamic signals are extensively used in resting-state fMRI studies to infer neural activity not driven by tasks or stimuli[1,2]. A cornerstone assumption of these studies is

Correspondence to: Patrick J Drew, pjd17@psu.edu, Department of Engineering Science & Mechanics, W-317 Millennium Science Complex, Pennsylvania State University, University Park, PA 16802.

Code Availability Code used to generate the figures in this paper is available at: https://github.com/DrewLab/Winder_Echagarruga_Zhang_Drew_2017_Code

Data availability

The data in this paper is available here: https://psu.app.box.com/v/Winder2017-Code-Data.

Author Contributions: ATW and PJD designed the experiments, ATW, CE and QZ performed experiments and analyzed the data, ATW and PJD wrote the paper.

Competing Financial Interests: The authors declare no competing financial interests.

that spontaneous hemodynamic signals are coupled to neural activity in the same manner as hemodynamic signals elicited by sensory stimuli. Recent studies have cast doubt on the one-to-one coupling of neural activity to hemodynamic signals during sensory stimulation[3–5], making it critical to determine how spontaneous hemodynamic signals are coupled to neural activity. To determine what aspects of neural activity are reported by spontaneous hemodynamic signals during different states, we simultaneously measured neural activity[5] and cerebral blood volume (CBV), using intrinsic optical imaging[4–6] in the vibrissa cortex of awake, head-fixed mice[7,8] (Figure 1a,c,S1a) while monitoring whisker and body movements. Increases in CBV, which show up as *decreases* in reflectance (ΔR/R) in intrinsic optical imaging signals, are caused by arterial and capillary dilations[7,9,10] and lead to increases in oxygenation which can be detected with BOLD fMRI[11,12]. Although our optical signals originated from the superficial layers, CBV changes have similar dynamics and amplitudes throughout the depth of cortex[13], and CBV increases are tightly related to BOLD fMRI signals[14].

Results

Behavior drives spontaneous hemodynamic fluctuations

Since humans and animals continuously engage in small bodily motions[15,16] and actively sense their environment[17], we monitored body movement and whisker position to detect periods of active behavior and rest (Figure 1f, S1b). We obtained an average of 254±54 minutes of simultaneous CBV, neural, and behavioral data from each mouse (n=12, Figure 1b). We categorized the data into several states: stimulation of the whiskers (contralateral to the window) with brief, gentle puffs of air directed towards the whiskers but not the face[7], volitional whisking, and rest (Figure 1b,f see methods). Periods of time greater than 10 seconds in duration without stimulation where the animals did not volitionally whisk were defined as true ‘rest’. Periods of rest lasting less than 10 seconds were considered as transitions between behaviors, and were omitted from subsequent analyses. Extended (>2 seconds) volitional whisker movements were analyzed separately from brief volitional movements since they were generally associated with additional body motion and distinct vascular responses[13]. We also used auditory stimulation (air puffs aimed away from the body) and stimulation of ipsilateral whiskers, but as these stimuli primarily elicited volitional whisking behavior (Figure S1h), we focus below on rest, volitional whisking, and stimulation of the contralateral whiskers in subsequent analyses.

We first asked if there were any differences in the amplitude of hemodynamic fluctuations across these different states, as non-stationarities in variance have been postulated to account for most of resting-state connectivity[18], though this non-stationarity has been argued to be spurious and driven by head movement and/or sampling variability[19]. As our signals are unaffected by head motion, and as we can parse our data into identified behavioral epochs, we can directly address this issue in our system. The variance of hemodynamic signal fluctuations in our mice was significantly and substantially larger during all of these states than at rest (Figure 1e). These result show that, in the awake brain, active sensation and volitional movements drive substantial changes in hemodynamic signals, and variability in the amount of these behaviors will contribute to the large trial-to-trial variability observed in

hemodynamic signals 'at rest'[20]. While our observation that the variance in the CBV signal differed among behavioral states does not rule out statistical or head-motion related artifacts in generating or contaminating dynamic connectivity patterns seen in human fMRI[19], it shows that the amplitude of spontaneous hemodynamic signals will be affected by behavioral state

Correlations between spontaneous neural activity and CBV changes

We then examined what aspect of neural activity was correlated with the observed CBV changes. Electrophysiology is considerably more sensitive to low levels of neural activity than calcium imaging, which fails to detect a substantial portion of the action potentials, particularly at low firing rates[21], and which cannot detect local field potential (LFP) oscillations. Consistent with previous measures showing a relatively tight spatial relationship between CBV changes and neural activity[6], we observed that the measured reflectance from pixels near the stereotrode recording site was correlated to the multi-unit average (MUA, a measure of local spiking) during periods of rest in all animals (Figure 1d). Passive sensory stimulation and volitional whisking both evoked increases in the gamma-band power (40–100 Hz) of the LFP, low-frequency power (<5 Hz) of the LFP, MUA, and CBV (Figure 2a,b), similar to responses in the visual system of primates[4,22], however the MUA response to whisker stimulation and volitional whisking varied among animals[23]. The heart-rate increase induced by the sensory stimulus was small (2.2±1.3%, Figure S2c,e), and the CBV responses were localized to the histologically reconstructed vibrissa cortex and the adjacent multisensory area[24] (Figure S1i). The sensory-evoked CBV-increase was not altered in mice with facial nerve transections, which prevented whisking (Figure S3a), showing that stimulus-elicited whisking had a negligible effect on the sensory-evoked CBV response[25]. During periods of rest, power increases in the gamma-band[20] and the MUA were consistently correlated with CBV increases (Figure 2c, S4). The correlations between neural activity and CBV in the absence of sensory stimulation were not substantially affected by facial motor nerve transection (Figure S3b,c), demonstrating that these spontaneous fluctuations in neural activity were centrally generated, not re-afferent signals.

Neurovascular coupling was similar across behavioral states

We first tested if neurovascular coupling was similar across different states (sensory stimulation, volitional whisking, and rest). To quantitatively compare the relationship between neural activity and CBV, we calculated the hemodynamic response function (HRF)[4,9,26], which is the kernel that relates neural activity to subsequent changes in blood volume. We selected an ROI around the electrode (mean area±std:0.6±0.1mm^2) based on the resting CBV-MUA correlation map and location of vibrissa cortex (see Figure 1d and Methods) to maximize the likelihood of obtaining a strong correlation between neural activity and CBV during rest. We compared HRFs calculated from neural and hemodynamic data, segregated by behavioral state, in order to determine whether behavior modulated the relationship between neural activity and subsequent changes in CBV. Because both sensory-evoked and spontaneous increases in CBV were most strongly and consistently correlated with gamma-band and MUA-band power during rest[20] (Figure 2c, see also S4), we focused our analysis on these neural measures. Across all states, the HRFs showed that increases in gamma-band power and MUA drove a decrease in reflectance (increases in CBV) with

similar latency (Figure 2d,e, S5a,b), indicating that the temporal dynamics of the hemodynamic response was not different across behavioral states. The similarity of overall dynamics (time to peak, full width at half maximum) for all conditions implies that neurovascular coupling was constant across behaviors. The shapes of the HRFs were similar regardless of electrode depth (Figure S1g, S5c,d).

Predicting the hemodynamic response from neural activity

We then asked how well the CBV signal could be predicted using neural activity for each type of behavior, which bears on the 'decoding' of fMRI signals[27]. By neural activity, we mean the electrical activity of neurons (action potentials, and the summed action of EPSPs and IPSPs that generate fluctuations in the local field potential) that generate multiunit average and LFP signals, and when blocked in a brain region perturb sensory perception[28] or motor behavior[29], not the basal metabolic processes that reflect housekeeping functions[30] and that persist in the vegetative coma state. Using HRFs which correspond to each type of behavior, we predicted the stimulation- or volitional-whisking-triggered *average* CBV response using the stimulation- or volitional-whisking-triggered *average* neural response, and then calculated the coefficient of determination (R^2) between the actual and predicted CBV responses[4] (Figure 3a,c,d, S6, S7a,b, see Methods). Because the neural and CBV signals must be time-locked to an event for averaging, this cannot be done for resting data. We observed a strong agreement between our prediction and the actual average CBV response to vibrissa stimulation using gamma-band power derived HRFs (median ±interquartile range: R^2=0.77±0.24), which was as good as previous measures of neurovascular coupling in the visual cortex of primates[22,31,32]. We also observed a reasonably good agreement between predicted and actual CBV responses to volitional whisking (median±interquartile range: R^2=0.21±0.25). These HRFs were then used to predict CBV fluctuations on individual stimulation, volitional whisking, and rest trials in order to determine how much of the ongoing CBV could be explained by neural activity. In comparison to the averaged data, the median R^2 of the CBV prediction over individual trials was substantially lower for all behavioral conditions when predicting ongoing CBV changes (Figure 3c,d). A sliding window was used to visualize time-varying differences in prediction accuracy on a second-by-second basis during an episode containing sensory stimulation, volitional whisking, and rest. This result showed that prediction accuracy was higher during periods containing large CBV fluctuations (such as would be seen during sensory stimulation or movement, see Figure 1e) (Figure 3b,c,f, S7f,g). CBV changes predicted from gamma-band power during rest were poor predictors of the actual CBV fluctuations (mean ±st. dev: R^2=0.06±0.03), and predicted significantly less CBV variance than predictions made from MUA during rest (mean±st. dev: R^2 = 0.14±0.09; Figure 3e). The low R^2 was not due to the quality of HRFs, since the HRF captured the majority of the averaged stimulus-triggered CBV variance (Figure 3a,c,d). Lower-frequency bands (0.1–8 Hz and 10–30 Hz) of the LFP were essentially uncorrelated with resting hemodynamic signals (median R^2<0.02 for both frequency bands, Figure S6). Additionally, when animals were more behaviorally active, the CBV predicted from neural activity was in good agreement with measured CBV changes (Figure 3f). The disagreement between the predicted and actual CBV on an event-by-event basis was not due to instrumentation noise (Figure S1d,e), and spontaneous CBV fluctuations were not substantially correlated with fluctuations in heart-rate (Figure S2g),

ruling out a systemic cardiovascular origin[33]. Lastly, subtracting off the global hemodynamic signal within the window (Figure S7e) does not substantially improve the quality of the prediction, indicating that the signals are not generated by global blood-volume fluctuations but rather have complicated spatiotemporal dynamics (Supplementary Movie 1). These results show that the hemodynamic response was strongly coupled to the gamma band of the LFP and the MUA when neural activity was high, regardless of the source of the neural activity, but the correlation broke down when neural activity was low, such as during rest.

Separate, additive components within the hemodynamic signal

What could account for the much lower correlation between the predicted and actual CBV for individual events versus the average and the poor performance of the HRF in predicting CBV fluctuations during rest? As our predictions of sensory-evoked CBV changes from neural activity were consistent with previous primate studies[4,20,22,32] (see Discussion), and performed well during behaviors with large modulations of neural activity (Figure 3f), it seems unlikely that the weak correlations between neural activity and CBV changes at rest could be due to our experimental conditions. We hypothesized that there are *two* processes that underlie local CBV changes: a neuronal source that drives vasodilation when neurons are active[34], and a second component which is uncorrelated to the measured local neural activity and that additively interacts with the neural-evoked CBV component (Figure 4a). In this model, the additional CBV component would be removed by averaging over stimulus presentations, since the timing of neural events will be random with respect to the phase of these uncorrelated CBV fluctuations. This hypothesis accounts for the substantially better predictions of behavior-averaged CBV changes from neural activity compared to individual events. In addition, the larger neural responses to sensory stimulation (versus volitional whisking or rest) will increase the amplitude of the neural-evoked hemodynamic signal with respect to the putatively non-neuronal component. The increased amplitude of the neural-evoked CBV would also increase the fraction of the signal that can be predicted from neural activity, and account for the differences in HRF performance in predicting CBV changes from neural activity among behaviors (Figure 3c,d, S7f,g).

Our hypothesis makes two testable predictions. First, the two CBV components should combine additively, so that the residuals (corresponding to the portion of CBV uncorrelated with local neural activity) of the predicted CBV should have constant amplitude across states. To test for additivity, we compared the CBV variance around the mean stimulus-evoked and whisking-evoked response to the CBV variance at rest. We found that the CBV variance during rest was not different from the trial-to-trial variance during behavior (Figure 4b). The same pattern holds true when we subtracted the neural-evoked CBV component (predicted using either the gamma-band and MUA derived HRFs), from the measured CBV signal for each of the behavioral conditions and calculated the variance of the residuals. The level of putatively non-neuronal noise was roughly constant across conditions, as the ratio of the residuals during sensory-evoked and volitional non-neuronal periods to those during rest (as measured by the root-mean squared error (RMSE) between the predicted and actual CBV signal) was close to 1 (Figure 4c,d). The additive noise hypothesis also predicts that CBV should be better predicted by neural activity during periods with greater modulation of

spontaneous (non-experimenter evoked) neural activity, which we also see in our data (Figure S7f,g,h). These analyses support the hypothesis that there are two additively interacting components of the CBV, one of which is linked tightly to the measured neural activity.

Origin of spontaneous hemodynamic fluctuations

There are several mechanisms which could give rise to the component of the CBV signal that was not predicted by our measures of neural activity. One possibility is that it could be local or distant groups of neurons whose activity is not detectable in the LFP/MUA, but can elicit a vasodilatory response, which we test below. Examining the power spectra of the predicted and actual CBV changes over the entire trial (Figure S7c), we see the largest difference in the 0.1–0.3 Hz frequency range, and the power spectrum of the HRF prediction error during periods of rest (Figure S7d) shows a similar peak at 0.2 Hz[35]. The spectral power of the residual CBV indicates that it is unlikely that the spontaneous activity of astrocytes drives these additive CBV oscillations because the spontaneous calcium signals in cortical astrocytes are nearly a *hundred* times slower than the CBV fluctuations we see here (0.1–0.3 Hz vs. 0.005 Hz)[36]. However, the CBV fluctuations could be due to intrinsic oscillations in the membrane potential (and contractility) of the smooth muscle around arterioles that additively interact with vasodilatory signals from neurons, similar to the way intrinsic membrane oscillations can sculpt response dynamics in neurons. Vascular oscillations are plausible mechanism for the persistent CBV changes because isolated arterioles show spontaneous fluctuations in their membrane potential and diameters in the same frequency range that we observed in the residual of our CBV prediction[37]. Vessel diameter is linearly related to smooth muscle membrane voltage so long as the vessel is not maximally dilated[38], and our stimulus-induced dilations are in this linear regime (9% peak arteriole dilation to punctate contralateral vibrissa stimulation[7] vs. >40% maximum arteriole dilation[39]). In contrast to neural-evoked fluctuations, fluctuations of a vascular origin should persist when neural activity is silenced.

We tested whether silencing local spiking blocks spontaneous CBV fluctuations during rest by infusing muscimol into the cortex via a chronically implanted cannula. The efficacy of the muscimol infusion was monitored with a stereotrode placed 1.5±0.5 mm from the cannula (Figure 5a, S1g, S8a). A semi-circular ROI centered on the cannula and with a radius specified by the distance between the electrode and cannula, was selected to ensure that the ROI only included silenced cortex. Since we observed clear suppression of neural activity with electrodes placed ~2 mm away, the infusion should affect all cortical layers (as the cannula was placed ~200μm below the surface, and the mouse cortex is ~1.2 mm thick).

Muscimol infusion caused a strong decrease in the sensory-evoked and baseline MUA, as compared to control aCSF infusions (Figure 5b, S7i, S8a, S9a). Similarly, the standard deviation in the MUA signal during periods of rest was decreased by 95±2% of the control (see Methods), indicating a nearly total silencing of spontaneous local spiking (Figure 5g). The standard deviation of gamma-band power was reduced by 73±15% (Figure 5j). If resting hemodynamics arose primarily from local spiking, then the spontaneous fluctuations in CBV should show profound reductions in amplitude, essentially disappearing. However,

all animals showed a significant and substantial remaining CBV fluctuations during periods of rest, despite the nearly complete reduction of local neural activity (resting CBV root mean-squared amplitudes after muscimol infusions were 84±41% of aCSF infusions, 95% confidence interval: [62–112%], bootstrap of the population mean, 2000 resamples, Figure 5c,d,g,j, S8a). Muscimol infusions did not appreciably change the spatial patterns of the resting CBV fluctuations or the spectral power of the oscillations compared to the HRF prediction residuals (Supplementary Movie 2,3; Figure S7d).

We also measured the diameters of arterioles after local infusion of aCSF or muscimol using 2-photon microscopy[7,39]. We measured from arterioles that would be well within the silenced region (mean vessel distance from infusion cannula: 0.75±0.14 mm). These single arteriole measures also showed small decreases in normalized fluctuation amplitudes at rest after muscimol infusions relative to aCSF infusions (resting root mean squared diameter fluctuations after muscimol infusions were 80±25% of aCSF infusions, mixed-effects ANOVA, p=0.0015, t(36)=3.43, n=19 pial arterioles in 4 mice; 71±30%, n=8 penetrating arterioles in 2 mice; p=0.36, t(14)=0.94) (Figure 5d,e). These results indicate that at least half of the resting CBV fluctuations were not directly linked to local neural spiking.

Several studies have suggested that pre-synaptic activity alone, in the absence of post-synaptic spiking, is sufficient to drive the hemodynamic response[12,40,41]. Hence, the remaining CBV oscillations could arise from glutamatergic release from distant cortico-cortical or subcortical projections, which would not be blocked by the local muscimol infusions. To determine whether presynaptic activity of long-range glutamatergic projections could account for the rest of the CBV oscillations through ionotropic receptors, we infused a cocktail of muscimol and ionotropic glutamate receptor antagonists, 6-cyano-7-nitroquinoxaline-2,3-dione (CNQX) and (2R)-amino-5-phosphonopentanoic acid (AP5), which inhibit AMPA and NMDA receptors, respectively (n=4, see methods). We again observed a strong reduction in the local multi-unit activity (96±2%, Figure 5h) as well as strong reduction in gamma-band power (87±9%, Figure 5k, S8b, S9b). However, the reduction in CBV amplitude oscillations at rest (40±20%, Figure 5h,k) was not significantly lower than the muscimol-only infusion, and did not account for the CBV or arteriole diameter oscillation (Figure 5f, 12±47% reduction, n=18 vessels) that remained in the absence of local neural activity. These results indicate that though presynaptic activity may contribute to some aspect of the spontaneous CBV fluctuations at rest, a large portion of the CBV fluctuations were not driven by either pre-synaptic neural activity or post-synaptic spiking.

Another possibility is that the remaining resting CBV fluctuations are driven by non-glutamatergic modulatory input[12,42], particularly noradrenergic input, as it has been shown in human studies[43] to play a role in resting state signals. To determine whether adrenergic input drives the remaining CBV oscillations after silencing local neural activity, we infused a cocktail of muscimol and adrenergic receptor blockers prazosin, yohimbine, and propranolol. The infusion of this cocktail again suppressed local spiking (94±5%, n=5, Figure 5i, S8c, S9c) and gamma-band power (79±15%, Figure 5l), and reduced the amplitude of the CBV fluctuations by 40±17%, though not significantly lower than the infusion of muscimol alone. These data indicate that there was minimal contribution of

adrenergic signaling to generating the ongoing CBV fluctuations in the absence of local spiking.

Because the cells in the vasculature are electrically coupled, there is a possibility that dilations in distant areas could propagate into the silenced region, which has been seen before in visual cortex[44]. To determine whether propagation of vascular dilation could account for the observed CBV changes in the silenced region, we calculated the cross-correlation between CBV fluctuations within the ROI and the rest of the window from data taken after the infusion of muscimol and aCSF. If propagation of dilation accounts for the remaining CBV fluctuations, the correlation coefficient between these regions should increase, and the time-lag at which maximum correlation occurs should be delayed following muscimol infusion. We found that neither the correlation or lags were significantly different between aCSF and muscimol trials. This indicates that the remaining CBV fluctuations did not propagate from other regions within the window[44] (Figure S10). Taken together, these results indicate that resting CBV consists of contributions from local neural populations, but that at least half of the resting CBV amplitude is not due to local neural processing, glutamatergic input, or adrenergic modulation. This remaining CBV oscillations had most of their power between 0.1–0.3 Hz, which is spectrally indistinguishable from neural evoked CBV (Figure 4a, S7d), and were uncorrelated to sensory stimulation and movement (Figure 4b,c,d).

Discussion

Comparison to previous measures of spontaneous and sensory-evoked neurovascular coupling

The correlations between neural activity and CBV we observed in the absence of sensory stimulation agreed well with those obtained in awake monkeys (see Figure S4, mean±std: r=0.21±0.07 vs. Schölvinck et al. 2010[20]: 0.2<r<0.3). We found a median R^2=0.77 for our gamma-band power derived prediction of stimulus-triggered average CBV, comparable to previous work in anesthetized primates (Logothetis et al. 2001[31], R^2=0.76, 0.9 reported for two different experimental sessions). Our trial-by-trial R^2 values for contralateral sensory stimulation were 0.34 and 0.30 for the gamma-band and multiunit average signals, respectively, very similar to those obtained by Goense et al.[22] in awake primates. It seems unlikely that we are missing a signal detectable by conventional electrophysiological techniques.

Comparison of our sensory-evoked HRF prediction accuracy to other studies needs to take into account the strength and duration of the stimulus used, and whether this is for averaged stimulus-evoked hemodynamic changes or calculated on a trial-by-trial basis. The visual stimulation in these previous studies produces substantially larger and more prolonged spiking activity increases than our whisker stimulation (Logothetis et al. 2001: 10 std above rest, stimulus 4–24 seconds duration; Goense et al., 2008, 8–10 std above rest, 15 seconds duration; Sirotin & Das 2009[4]:~400% above resting rates, ~5 seconds duration; this study: 3std/170% above rest, stimulus 10ms duration). Importantly, the R^2 between the actual and HRF-predicted CBV decreases as the stimulus intensity is reduced[32]. When we compare our results with stimuli that elicit comparable changes in neural activity with the awake primate

data (low contrast (~12.5%) visual stimulation in Cardoso et al. 2012: ~200% increase; this paper: 170% increase), we are in good agreement (R^2 values: Cardoso et al. 2012: 0.26, their supp. Figure 3; this paper: 0.31).

Recent work measuring cerebral blood volume and changes in GCaMP fluorescence in awake-head fixed mice during periods without locomotion, but no other behavioral monitoring, reported good agreement between CBV and fluorescence changes[45]. However behaviors, such as whisking, grooming (Figure 3f) and brief (<1 second) movement events[9,46] may contaminate these signals. Lastly, "ground truth" experiments that simultaneously measured spiking activity with electrophysiology and fluorescence of calcium indicators have shown that even the best spike-detection algorithms detect far fewer than half the spikes, and that this issue is worse at low firing rates, the regime where resting state activity is likely to be taking place[21].

Implications of potential non-neuronal signals for hemodynamic imaging

Our results have several important implications for the interpretation of the neural correlates of hemodynamic signals. We showed that 'spontaneous' hemodynamic signals are driven by behaviors, such as active sensing and small body movements, that are typically ignored in human and animal imaging studies. These movements drive spatially-localized hemodynamic signals and arterial dilations[5,39], and because of the spatial specificity of these hemodynamic changes, a global regression procedure will be ineffective in removing these movement-evoked activations, and may even introduce artifacts[47]. Our results in particular call into question previous studies which used spontaneous hemodynamic signals to assay neural differences that accompany disease, aging, and other conditions, as slight differences in behavior could drive differences in spontaneous dynamics independent of any underlying differences in neural activity.

We demonstrated that unlike the sensory-evoked response, in the true 'resting-state', at least 50% of the CBV signal is unrelated to local cortical processing, glutamatergic input, or noradrenergic modulation. While our results are consistent with the idea that these uncorrelated fluctuations in CBV have a non-neuronal origin, we cannot completely rule out other possible origins. For example, the spontaneous fluctuations could be driven by a subpopulation of vasodilatory neurons[48] or the recruitment of local astrocytes[34] whose activity we cannot detect in the MUA/LFP. However, to account for the additive CBV signal, any driver must have activity that is completely uncorrelated with other neurons, and have activity patterns are unaffected by sensory stimulation or behavior. Additionally, for this alternative hypothesis to be true, when all of the vasodilatory input to the blood vessels is silenced during the local pharmacological infusions, the arterioles would need to have a homeostatic process that drives similar oscillations in diameter when the neural input is removed. To our knowledge, there are no such candidate neurons or processes in arteries. However, we hope that these results will motivate further investigations in to the details of neurovascular coupling and smooth muscle biophysics[34]. If these persistent CBV oscillations are of vascular origin, their function is not clear, though vascular pulsations have been implicated in driving fluid exchange in the glymphatic system[49].

Whatever the origin of the spontaneous CBV oscillations, our results clearly show that in the absence of overt stimulation or behavior, hemodynamic signals are very poorly correlated with any conventional measure neural activity (Figure 3). This poor correlation is in direct contrast to sensory- and behaviorally-evoked hemodynamic signals, which are relatively tightly coupled to the underlying neural activity. Subtracting off the global signal (Figure S7e) did not substantially improve this correlation, suggesting that there is no simple fix. Because of technical considerations, BOLD fMRI signals will have even lower correlations with neural activity than the CBV signals we record here[11], making the problems observed here even *more* acute for human studies. This 'noise' will limit the ability to detect and accurately infer the ongoing neural activity, and can only be surmounted by massive averaging. However, we note that these results do not refute the existence of functional connectivity, which have been validated using direct assays of neural activity[50].

In light of these results, we propose fundamental changes in the way resting-state studies should be performed and interpreted. First, it is essential to measure behavior in a very detailed way during imaging to ensure that behavioral variability does not drive differences in spontaneous activity between groups or across conditions. Small differences in the frequency of active sensing behaviors and movements will drive large differences in spontaneous hemodynamic signals. Secondly, during periods of true 'rest', hemodynamic signals should not be interpreted as being solely driven by electrical activity in neurons. Rather, these signals have contributions from other processes which are additive to, and uncorrelated with, neurally evoked CBV changes.

Methods

Animals Procedures

All procedures outlined below were in accordance with guidelines from the Institutional Animal Care and Use Committee (IACUC) of Penn State. Data were acquired from 42 (12 for HRF and behavior measurements, 3 for window-only controls, 3 for transected motor nerve controls, 7 for two-photon laser scanning microscopy (2PLSM), and 17 for cannula implantation and infusion experiments) male, C57-BJ6 mice (Jackson Laboratory) between 3–8 months of age. Mice were given food and water ad libitum and maintained on 12-hour light/dark cycles in isolated cages during the period of experiments. All imaging took place during the light cycle period. Sample size was chosen to be consistent with previous studies[6–9]. Data collection and analysis were not performed blind to the conditions of the experiments. Drug infusions were counter-balanced across animals. See the "Life Sciences Reporting Summary" for more details.

Surgery

Electrode, cannula, and window implantation procedure for Intrinsic Optical Signal (IOS) imaging experiments—Mice were anesthetized with 2% Isoflurane (in oxygen) for all surgical procedures. A custom-machined titanium metal bar, used to fix the mice in place during imaging, was attached to the skull with cyanoacrylate glue (Vibra-Tite, 32402). The bar was positioned along the midline and just posterior to the lambda cranial suture. A reinforced thinned-skull window was created over the left hemisphere as described

previously[5,51]. A 4–10 mm^2 area of skull was thinned over the whisker representation of somatosensory cortex (Figure 1c,d). A Teflon-coated tungsten-wire (AM systems, #795500) stereotrode was inserted into the barrel cortex at 30–45 ° from the horizontal along the rostral/caudal axis using a micromanipulator (Sutter Instruments, MP285) through a small hole made at the edge of the thinned area, so that the electrode tips were within the window (Figure 1c). The hole was sealed with cyanoacrylate glue. In a subset of mice (n=17), a small craniotomy was made at the edge of the thinned area of skull and a cannula (Plastics One, C315DCS, C315GS-4) was inserted into the upper layers of cortex (Figure 5a, S1g, S8). The cannula was attached to the skull with cyanoacrylate glue and dental acrylic. The thinned area of skull was reinforced with a fitted #1 glass coverslip (Electrode Microscopy Sciences, #72200). Three self-tapping, 3/32″ #000 (J.I. Morris) screws were inserted into the contralateral parietal and frontal bone and ipsilateral frontal bone. A stainless-steel wire (A-M Systems, #792800) was wrapped around the screw implanted in the frontal bone contralateral to the window for use as an electrical ground for neural recordings. The titanium bar, screws, and tungsten wires were secured with black dental acrylic resin (Lang Dental MFG. Co., REF 1530) to minimize light reflection. The animals were allowed to recover for 2–3 days before habituation. Neither electrode nor cannula implantation affected the hemodynamic response (Figure S1f).

Cannula and window implantation for two-photon laser scanning microscopy (2PLSM)—As above, mice were anesthetized with isoflurane for all surgical procedures. A titanium head bar was placed as described above, and a 4–6 mm^2 polished and reinforced thinned-skull window was created over the forepaw/hindpaw representation of somatosensory cortex of the left hemisphere[51]. After polishing the skull with 3F grit (Covington Engineering, Step Three 3F-400), a small craniotomy was made to insert the cannula into the upper layers of cortex near the forepaw/hindpaw representation of cortex. The thinned area of the skull was reinforced with a fitted #0 glass coverslip (Electrode Microscopy Sciences, #72198). Two self-tapping screws were inserted into the contralateral parietal and ipsilateral frontal bone. The titanium bar, cannula, and screws were secured with black dental acrylic resin. The animals were allowed to recover for 2–3 days before habituation.

Facial nerve transections—Animals were anesthetized with 2% isoflurane and bilateral incisions were made posterior to the whisker pad. The facial nerve was transected with iris scissors[25] and the incisions were sutured. Topical antibiotic ointment was applied (Neosporin), and animals were allowed to recover for 2–3 days before habituation to head fixation. Animals were monitored to verify that no vibrissa movement occurred following transection.

Histology

At the end of the experiment, animals were deeply anesthetized with 5% isoflurane. The mice were transcardially perfused with heparinized saline and then fixed with 4% paraformaldehyde. Fiduciary marks were made in each of the corners of the cranial window. The brains were extracted and sunk in a 30% sucrose/4% paraformaldehyde solution. The flattened cortexes were sectioned tangentially (60 μm per section) using a freezing

microtome and stained for the presence of cytochrome-oxidase (CO). Whisker barrels were visible in layer IV of CO stained sections, allowing the alignment of the windows and stereotrodes with respect to the barrel cortex[52,53]. The laminar location of the stereotrodes were categorized as supragranular, granular, or infragranular by identifying the first cortical section without visible electrode tracks relative to sections showing whisker barrels.

Physiological measurements

Data from intrinsic optical signal and electrophysiology experiments were acquired with custom LabVIEW program (ATW and PJD, version 11.0, 64-bit Windows 7, National Instruments, Austin TX). Data from 2PLSM experiments was acquired using the Sutter MCS software (Sutter Instruments, Novato, CA). All experiments were performed with mice in sound-attenuating boxes.

Habituation—Animals were gradually acclimated to head-fixation and stimulation over three habituation sessions. Mice that received whisker stimulation (n=31) were acclimatized to head-fixation for 15–30 minutes during the first session. In the subsequent sessions, they began to receive air puffs directed at the whiskers, and were head-fixed for longer durations (>60 minutes). Mice which were imaged using 2PLSM (n=7) were acclimated to the spherical treadmill (60 mm radius) over 3 days. During the first session, they were head-fixed for 15 minutes. On subsequent days, the time was increased to ~60 minutes. Mice were monitored for any signs of distress during habituation. In all cases, the mice exhibited normal behaviors such as exploratory whisking and occasional grooming after being head-fixed. Heart rate-related fluctuations were detectable in the intrinsic optical signal (see below) and remained between 7–14 Hz for all mice during and after habituation. This is near the mean heart-rate (~12 Hz) telemetrically recorded from mice in their home cage[54]. Experimental data were taken over 2–5 imaging sessions.

Intrinsic optical signal (IOS) imaging—Twenty minutes before the experiments, the mice were briefly (<1 minute) anesthetized with isoflurane (5%), and fixed into the imaging apparatus using the attached titanium head bar. When fixed, the animal's body was supported in a clear plastic tube (n=31), or on a ball (n=4). The imaging apparatus and head-fixing apparatus were arranged to avoid incidental whisker contact during whisking. Blood volume was measured by illuminating the cranial window with three collimated and filtered 530±5 nm LEDs (Thor Labs, FB530-10, M530L2). This wavelength is an isobestic point of the hemoglobin light absorption curves. Reflected light intensity from the surface of the brain at this wavelength gives a measurement of the total hemoglobin concentration which we used as a measure of cerebral blood volume. Decreased reflectance from the cranial window corresponds to increased absorption by hemoglobin due to increased CBV. The cranial window was imaged with a Dalsa 1M60 Pantera CCD camera (Phase One, Cambridge MA) positioned directly above the mouse. Light entering the camera was filtered using a mounted green filter (Edmund Optics, Barrington NJ, #46540) to block the light used for whisker tracking. Images (256×256 pixels, 15 μm per pixel, 12-bit resolution) were acquired at 30 Hz[9,55]. The data was then low-pass filtered (3 Hz, Butterworth, order=4, MATLAB function: butter, filtfilt) to remove heart-rate related fluctuations.

Electrophysiology—Neural activity was recorded simultaneously with the IOS as differential potentials between the two leads of Teflon-insulated tungsten micro-wires (A-M Systems, #795500)[5]. Stereotrode micro-wires, with an inter-electrode spacing of ~100μm, were threaded through polyimide tubing (A-M Systems, #822200). Electrode impedances were between 70–120 kΩ at 1 kHz. The acquired signals were amplified (World Precision Instruments, DAM80), band-pass filtered between 0.1 and 10 kHz (Brownlee Precision, Model 440) during acquisition, then digitized at 20 kHz (National Instruments, Austin TX, PCI-6259). We were able to detect individual spikes in all animals (Figure S1c), however the spiking response to whisker stimulation and volitional whisking varied among animals[23]. We quantified spiking activity using the multi-unit average (MUA), which is the power of the signal within the 300–3000 Hz band[22]. Power was calculated by digitally band-pass filtering the raw neural signal (MATLAB function: butter, filtfilt; filter order = 4). The result was squared, low-pass filtered below 10 Hz, and resampled at 30 Hz. A baseline power (P_b) was computed by averaging the band-limited power during periods of the imaging session where no stimulation or volitional movement occurred. The normalized power was then calculated to be $\Delta P/P_b = [P-P_b]/P_b$. Gamma-band power was calculated in the same manner using the 40–100 Hz band of the LFP. Neither the LFP nor the MUA signals showed significant changes in sensory evoked amplitude (gamma-band power: p=0.94, t(61)=0.08; MUA: p=0.19, t(61)=1.33) or neural variance (gamma-band power: p=0.81, t(61)=2.45; MUA: p=0.28, t(61)=1.09) from day to day (n=63, iteratively reweighted least squares, bisquare weighting, MATLAB function: robustfit), indicating that the recordings were stable across imaging sessions. The spatial resolution of the LFP depends on the distance between the recording electrodes. Differential recordings will sample the volume of tissue spanned by the electrodes, and if these electrodes are closely spaced[56,57], they will provide a very localized (equivalent to the electrode spacing) measure of the LFP. Using a remote reference can contaminate the LFP signal if activity in the remote area is non-stationary, as will be the case in an awake animal. Signals from spiking activity will be much more localized, and our electrode will record neural activity from a sphere of ~100μm in diameter[58]. For infusion experiments, band-limited neural power was normalized to the mean amplitude during periods of rest from the same session *prior* to infusion.

Two-photon microscopy—Mice (n=7) were briefly anesthetized with isoflurane and retro-orbitally injected with 50 μL 5% (weight/volume) fluorescein conjugated dextran (70 kDa; Sigma-Aldrich)[59,60] then fixed upon a spherical treadmill (see behavior tracking section below). Imaging was done on a Sutter Movable Objective Microscope with a 20× 0.9NA objective (Olympus). A MaiTai HP laser tuned to 800 nm was used for fluorophore excitation. Individual arteries (n=19 pial, 5 vessels/mouse; n=8 penetrating, 2–3 vessels/mouse) were imaged at nominal frame rate of 8 Hz for 5 minutes using 10–15 mW of power exiting the objective. The same arteriole segments in the limb representation of somatosensory cortex were imaged after aCSF and muscimol infusions.

Vibrissa stimulation—Animals were awake and engaged in whisking behavior during IOS data acquisition. Brief (0.1 second duration) puffs of air were delivered to the ipsilateral and contralateral whiskers[7] through a thin plastic tube (length 130mm, diameter 2mm). Air puffs were directed to the distal ends of the whiskers at an angle parallel to the face to

prevent stimulation of other parts of the head or face. An additional air puffer was set up to point away from the body for use as an auditory stimulus. The puffs were delivered via solenoid actuator valves (Sizto Tech Corporation, 2V025 1/4) at constant air pressure (10 psi) maintained by an upstream regulator (Wilkerson, R03-02-000). Air puffs were separated by an interval of 10–60 seconds, and the order of all sensory stimulation was randomized with a nominal ratio of 3 contralateral stimuli for every ipsilateral or auditory stimulation. Auditory and ipsilateral stimuli were omitted from the principal analysis because their responses were primarily related to stimulus-provoked movement (see figure S1h).

Behavioral measurement—For IOS imaging experiments, the whiskers contralateral to the imaged hemisphere were diffusely illuminated from below with 625 nm light (Edmund Optics, #66-833) and imaged using a Basler A602f camera (Edmund Optics, Barrington NJ) at 150 frames per second. The imaging region was restricted to the area just adjacent to the face with the long axis of the image parallel to the line of the face where whiskers curvature is minimal and the full range of whisker movement could be captured. As additional behavioral measurements, the animal was monitored using a webcam (Microsoft LifeCam Cinema^{TM}), and a force sensor (Tekscan, Flexiforce A201, Boston MA) was placed below the clear plastic tube to detect body movement. A threshold was established by examining force measurements when each animal was clearly moving during the trial. Changes in force which exceeded the threshold were flagged as body movements by the animal.

For 2PLSM imaging (n=7) and for a subset of IOS experiments (n=4), mice were fixed using the attached head bar on a spherical treadmill with one degree of freedom[5,60]. The treadmill was coated with anti-slip tape and attached to an optical rotary encoder (US Digital, E7PD-720-118) to monitor rotational velocity. For mice on the treadmill, ball movements were used to detect animal behavior in lieu of whisker tracking in order to identify periods of rest.

Intracortical infusions—For IOS imaging, animals were placed in the imaging apparatus as described above. Ten minutes of CBV, neural, and behavioral data were acquired with the dummy cannula in place. The dummy cannula was then slowly removed and replaced with an infusion cannula (Plastics One, C315IS-4). The interface between the infusion cannula and the guide cannula was sealed with Kwik-Cast (World Precision Instruments). Muscimol (10mM)[61], a muscimol (10 mM) + CNQX (600μM) + AP5(2.5mM) cocktail, a muscimol (10mM) + prazosin (1mM) + yohimbine (1mM) + propranolol (1mM) cocktail[62], or aCSF were infused at a rate of 25 nL/minute for a total volume of 500 nL. CBV and neural activity were constantly monitored during the infusion to ensure that cannula placement did not affect neural activity or hemodynamic signals. Autoradiography[63], immunohistochemistry[64], and gene expression[65] studies have failed to detect GABA-A receptors in the small vessels of the cerebral vasculature whose dilations we measured here. Blocking GABA-A mediated transmission does not block optogenetically-evoked vasodilation by interneurons[66], indicating that GABA-A receptors do not mediate activity-evoked vasodilation. To validate that the cannula was patent, infusions were combined with 1% Fluorescein isothiocyanate (FITC). To verify successful infusion, FITC fluorescence was visualized by capturing images of the thinned skull window while being illuminated with blue light (470 nm, Thor

Labs, M470L2) every ~5 minutes. Pharmacological treatments and aCSF were each infused in a counter-balanced order. All mice received both infusions of drugs and an aCSF control, so no randomization was needed. Neural and CBV measurements were acquired during the infusion as an additional means of assaying the efficacy of pharmacological manipulation. Pharmacological data were only used if the MUA amplitude was confirmed to have decreased by >80% compared to aCSF. Baseline reflectance from the ROI increased as neural activity was increased, indicating decreased CBV. CBV baselines prior to this decrease were used for normalization. Some animals exhibited occasional bursts of neural activity accompanied by large CBV changes (10–15% peak to peak) approximately one hour after muscimol infusions. Data taken after a burst of activity were omitted from subsequent analyses. For 2PLSM imaging, mice were head-fixed on the spherical treadmill. Infusion cannulas were placed and infusions were conducted as described for IOS imaging, except FITC was not infused. Animals were kept in place for 20 minutes after the infusion and then moved to the imaging apparatus. The infusion cannulas were kept in place for the duration of the imaging session. Baseline diameter constrictions were observed during infusion, in accordance with intrinsic data. Vessel measurements occurred >45 minutes after the start of infusion.

Data Analysis

All analyses were conducted using custom-written code (ATW, CE, QZ, and PJD) in MATLAB 2015a (Mathworks).

Alignment of anatomical areas to CBV imaging data—The location of the thinned-skull window with respect to anatomical landmarks of the cortex was obtained by aligning the surface vasculature in the most superficial histological sections with the vasculature visible through the window during imaging. Deeper sections were aligned using fiduciary marks and penetrating vessels as landmarks. All image alignment was performed using affine transformations in Adobe Illustrator CS6 (Adobe Systems).

Detection and quantification of whisker motion—Images of whiskers during data acquisition were converted into a relative whisker position by applying the Radon transform (MATLAB function: radon) to each image. Peaks from the resulting sinogram correspond to a position and angle of whiskers in the image. The mean whisker angle was extracted by identifying the angle of the sinogram which had the largest variance in the position dimension[59]. The mean whisker position was digitally low-pass filtered (<30 Hz) using a 4th order Butterworth filter (MATLAB functions: butter, filtfilt). Whisker acceleration was obtained from the second derivative of the filtered position and binarized according the equation:

$$\delta(t)=H(|a_t|-a_c)=\begin{cases}1, & |a_t| \geq a_c\\ 0, & |a_t| < a_c\end{cases}$$

where a_t is the acceleration at time t, and a_c is the acceleration threshold. Whisker acceleration was used since it is directly related to the force on the whisker. The whisking thresholds were empirically defined for each animal by identifying whisker accelerations

that occur when the animal was clearly whisking. Similarly, periods of rest were identified where the animal was not making exploratory whisker movements to establish acceleration values during non-whisking periods. Any isolated acceleration values which fell between these thresholds were omitted from analysis. Ambiguous acceleration values which occurred within 0.5 seconds of a clear whisk were considered part of the bout of whisking.

2PLSM image processing—Individual frames from 2PLSM imaging were aligned using a rigid registration algorithm to remove motion artifacts in the x-y plane[7,39]. Visual inspection of movies indicated that there was minimal z-axis motion. A rectangular box was manually drawn around a short segment of the vessel and the pixel intensity was averaged along the long axis. Pixel intensity was used to calculate diameter from the full-width at half-maximum. Diameters of penetrating arterioles were calculated using the Thresholded in Radon Space (TiRS) algorithm[67]. Periods of rest were segregated by using locomotion events measured with the rotary encoder[9]. For each 5-minute trial, diameter measurements were normalized to the average diameter during periods of rest. The diameters were smoothed with a 3rd order, 15 point Savitzky-Golay filter (MATLAB function: sgolayfilt). During all resting periods, the spontaneous fluctuations were compared by calculating the normalized standard deviation from the average baseline diameter. The standard deviation of the fractional diameter changes after pharmacological infusion were normalized by the standard deviations after fractional diameter changes after aCSF infusion for the same vessel segment.

Heart rate detection—We tracked heart rates by calculating time-frequency spectrograms with a 2-second sliding window on the median window reflectance (Figure S2a, Chronux Toolbox version 2.11 function: mtspecgramc; http://chronux.org/)[55,68]. We took the derivative of the median window reflectance to reduce the 1/f trend in the spectrum before calculating the time-frequency spectrogram and to improve detection of peaks in spectral power. The heart-rate was identified as the frequency with the maximum spectral power in the 5–15 Hz band.

Behavioral state categorization—For analysis of HRF dynamics, data were separated into three behavioral categories: contralateral whisker stimulation, volitional whisking, and rest. The period (6 seconds) following an air puff to the contralateral whiskers was isolated provided that the animal was quiescent at the time of stimulation. Volitional whisking behaviors were defined as the period following a voluntary movement of the whiskers with at least 3 seconds of rest prior to the whisker movement. The duration of the movement was also tracked and separated into short (< 2 sec) and long (>2 sec) movements. Resting behavior was defined as the absence of stimulation or movement. Periods of rest lasting < 10 seconds were considered to be transitions between behaviors and omitted from the principal analysis. Data corresponding to whisker stimulation and volitional whisking were isolated beginning 4 seconds before and 6 seconds after behavior onset.

For 2-photon microscopy data (n=7) and a subset of IOS animals (n=4), behavior was categorized by monitoring movement on a spherical treadmill with one degree of freedom[5,46]. Movement events were detected by applying a 5^{th} order low-pass filter (10 Hz, Butterworth, MATLAB function: butter, filtfilt) to the velocity signal measured by the

velocity encoder, taking the derivative of the velocity, and then comparing the absolute value of the resulting acceleration to a threshold of 10 cm/s^2 [9,39,60]. Periods of rest were categorized based on the binarized detection of the treadmill acceleration:

$$\delta(t)=H(|a_t|-a_c)=\begin{cases} 1, & |a_t| \geq a_b \\ 0, & |a_t| < a_b \end{cases}$$

where a_t is the acceleration at time t, and a_b is the treadmill acceleration threshold. Resting periods starting 2s (2PLSM) and 4s (IOS) after the end of any running event and lasting more than 10 seconds with no detected movement.

Region of interest selection and baseline—An ROI for each mouse was created by identifying image pixels within the barrel cortex that were correlated with neural activity when the animal was at rest. To identify correlated pixels, images of the thinned skull window and MUA data during periods of rest were chosen and normalized to the resting mean (Figure 1d, top left). The mean reflectance from the entire window at each time point (the global signal) was then subtracted from each pixel. The cross-correlation was calculated (MATLAB function: xcorr) between the reflectance signal of each mean-subtracted pixel and the MUA and normalized by the autocorrelations. The median correlation coefficients between lagged MUA (0.5–1.5 seconds, Figure 1d, bottom left) and the intensity of each pixel were plotted (Figure 1d, top right). This spatial correlation map was overlaid on a histological reconstruction of the window and electrode locations (Figure 1d, top left). In all animals, pixels with correlations between lagged MUA (0.5–1.5 seconds, see Figure 1d) and CBV greater than r=0.1 were adjacent to the stereotrode site and localized near the whisker barrels. A circular region of interest (ROI) was created to encompass pixels that were near the stereotrode, within the barrel cortex, and which showed positive correlations between the CBV signal and MUA at a 0.5–1.5 second lag (r>0.1) (ROI area: 0.6±0.1mm^2). For mice with an implanted cannula, regions of interest within the thinned-skull window were created by histologically identifying the location of the cannulas and stereotrodes and drawing a semicircular region with the cannula at the center and radius equal to the distance from the cannula to the electrode (Figure 5a, S8). Calculations of the reflectance baselines and normalization procedures were as described above. The ROIs of three animals spanned the window and were omitted from the analysis comparing the CBV within the ROI to the rest of the window.

Periods of rest were identified for each imaging session, and the mean intensity within the ROI was averaged over the duration of the resting data, giving a single reflectance baseline (R_b) for each animal and imaging session. The ROI reflectance was used as the measure of CBV for all experiments. The fractional change in ROI reflectance was given by $\Delta R/R_b = [R - R_b]/R_b$. For infusion experiments, only resting periods prior to infusion were used for normalization.

Triggered Spectrograms—Time-frequency spectrograms were calculated for the duration of the trial using multi-tapered spectral analysis (MATLAB Chronux toolbox version 2.11 function: mtspecgramc, www.chronux.org)[68]. The time bins surrounding

stimulation and whisking events were isolated and each frequency band was normalized to the resting baseline and then averaged over behavioral events.

Cross-correlation calculations—Neural signals were separated into frequency bands (~10 Hz resolution) within the LFP band by calculating the spectrogram (MATLAB Chronux toolbox version 2.11 function: mtspecgramc, www.chronux.org)[68] from periods of spontaneous or resting behavior lasting >10 seconds. Multi-unit activity (MUA) was defined as the power between 300 and 3000 Hz. Cross-correlograms were calculated (MATLAB function: xcorr) between the reflectance within the whisker barrel ROI and each frequency band and normalized by the autocorrelations. To directly compare our result against previous results obtained with interleaved electrophysiology and MRI-CBV imaging[20], the CBV and neural activity were both low-pass filtered below 1 Hz before calculating the cross-correlation.

Cross-correlations between heart rate and CBV were obtained during periods of rest lasting >10 seconds. Statistical significance computed using bootstrap resampling[69] from 1000 reshuffled trials.

Calculation of the hemodynamic response function—We considered the neurovascular relationship to be a linear-time invariant (LTI) system[26,32,70]. Using this framework, a hemodynamic response function (HRF) can be calculated numerically using the relationship:

$$H_{(k+1)\times 1}=(T^T T)^{-1} T^T V_{(m+k)\times 1}$$

H is the HRF, V is the normalized and mean subtracted cerebral blood volume (CBV), T is a Toeplitz matrix of size (m+k) · (k+1) containing measurements of normalized neural activity (*n*):

$$T(\vec{n})=\begin{pmatrix} 1 & n_1 & 0 & 0 & \cdots & 0 \\ 1 & n_2 & n_1 & 0 & \cdots & 0 \\ \vdots & \vdots & n_2 & n_1 & \cdots & \vdots \\ \vdots & n_k & \vdots & n_2 & \cdots & n_1 \\ \vdots & 0 & n_k & \vdots & \cdots & n_2 \\ \vdots & \vdots & \vdots & n_k & \ddots & \vdots \\ 1 & 0 & 0 & 0 & \cdots & n_k \end{pmatrix}$$

For calculations of behavioral HRFs, a subtractive normalization was performed so that the period of rest prior to behavior onset had a mean equal to zero. For sensory evoked HRFs, only neural activity within 1.5 seconds of the stimulus was used for calculating the HRF. For volitional whisker movement HRFs, we used a 4 second period of neural activity which began 1 second before the detected onset. This period includes any neural activity that precedes the onset of whisking or continues after super-threshold whisker movement has ceased.

HRFs were calculated from half of the data (described below) corresponding to each behavior, and tested on the other half. HRFs for each behavioral dataset were calculated from gamma-band power (40–100 Hz) and MUA power (300–3000 Hz) separately. All results were smoothed using a 3rd order, 11 point Savitsky-Golay filter (MATLAB function: sgolayfilt). Note that this method makes no assumptions as to the shape of the HRF, but nonetheless we recovered the canonical gamma-distribution function shaped HRF[71].

Comparison of HRF parameters among behaviors—Amplitude, time to peak, and full width at half-maximum were used as parameters to compare HRFs obtained from various behaviors. The HRF for each behavior was calculated for each animal. Population means (two-way ANOVA) or medians (Friedman test) were compared to determine the significance of any differences observed in the behavior-specific HRF attributes. Bonferroni corrections were applied to correct p-values for multiple comparisons in post-hoc tests. The dependence of HRF attributes on cortical depth was also examined. HRF attributes across all behaviors were separated by cortical electrode depth and compared non-parametrically using a Mann-Whitney U-Test.

Quantifying the variance in the CBV dynamics captured by the HRF—HRFs for each behavior were fit with a gamma-distribution function to calculate the correspondence between predicted and actual CBV. The gamma-distribution HRF was convolved with neural power to predict the measured CBV:

$$v = n \otimes h + \varepsilon$$

Where v was the predicted CBV, n was the normalized neural measurements, h was the HRF, ε was the error, and $\otimes$ denotes convolution. Data were separated into even and odd trials, spanning all imaged days. Even trials were used to generate the HRF, and odd trials were used to validate the HRFs predictions. The efficacy of the prediction was quantified by calculating the coefficient of determination (R^2) between the predicted and actual CBV:

$$R^2 = 1 - \frac{\sum (v_{actual} - v_{predicted})^2}{\sum (v_{actual} - \bar{v})^2}$$

where $\bar{v}$ is the expected value of the measured CBV. To test the hypothesis that fluctuations in R^2 were due to behavior, R^2 values from individual and average CBV predictions were compared using the Friedman test or ANOVA, as appropriate, with Bonferroni correction for multiple comparisons in post-hoc analysis.

Subtraction of the global CBV signal—To test the hypothesis that local CBV fluctuations arising from local neural activity may be obscured by a non-region specific "global" signal[72], we obtained the global signal by averaging the reflectance over the area of the thinned-skull window. We normalized the global signal to its baseline calculated, as described above, from periods of rest and subtracted the normalized global signal from the $\Delta R/R$ within the ROI in the barrel cortex. This subtraction preserved neurovascular coupling

(Figure 1d, S7e). We then repeated the calculation of the resting HRFs and predicted the measured reflectance after global signal subtraction (see Methods above).

Analysis of the putatively non-neural, additive CBV signal—Data were separated according to behaviors and normalized to the resting baseline. To determine whether the hypothesized CBV component might be uncorrelated, additive “noise”, we compared the variance of the behavior-triggered CBV response to the variance of the CBV signal during periods of rest (see Figure 4b). Additionally, we compared the root mean squared error of the gamma-band or MUA derived HRF predictions across all behavioral conditions (Figure 4c,d).

To examine the frequency content of the neurally-uncorrelated CBV component, the predicted CBV signal was subtracted from the measured CBV during periods of rest, and the multi-tapered power spectral density of the residuals were calculated (MATLAB Chronux toolbox version 2.11 function: mtspectrumc; http://chronux.org)[68] for each animal.

Statistics—Before statistical testing, sample populations were tested for normality (Anderson-Darling test, MATLAB function: adtest). If the distribution was not normal, the median±interquartile range was used to describe distributions instead of mean±standard deviation. For comparisons of multiple populations, the assumption of equal variance needed for parametric was also tested (two sample F-test, MATLAB function: vartest2, or Bartlett test, MATLAB function: vartestn). If the conditions of normality and equal variance were not met, parametric tests (t-test, paired t-test, Welch’s t-test, one-way anova, two-way anova) were substituted with a non-parametric counterpart (Mann-Whitney U Test, Wilcoxon signed-rank test, Kruskal-Wallis ANOVA, Friedman test). Wherever appropriate we accounted for within subject variations by using paired tests, two-factor ANOVA/Friedman test, or mixed-effects modeling[73] (MATLAB function: fitlme). Where n>10, the approximate method of Wilcoxon signed rank testing was used since signed ranks have a normal distribution, otherwise the exact sums of the signed ranks were used. All statistical comparisons were two-sided tests unless otherwise noted. Confidence intervals were obtained from bootstrap resampling (MATLAB function: bootci, 1000 resamples) from statistics calculated on randomly reshuffled data, where the size of the reshuffled data was equal to the original dataset.

Supplementary Material

Refer to Web version on PubMed Central for supplementary material.

Acknowledgments

This work was supported a Scholar Award from the McKnight Endowment Fund for Neuroscience, and R01NS078168, R01EB021703, and R01NS079737 from the NIH to PJD. We thank L. Abbott, M. Adams, P. Blinder, D. Feldman, and N. Zhang for comments on the manuscript, and J. Berwick, D. Kleinfeld, and C. Mateo for discussions

References

1. Fox MD, Raichle ME. Spontaneous fluctuations in brain activity observed with functional magnetic resonance imaging. Nat Rev Neurosci. 2007; 8:700–11. [PubMed: 17704812]
2. Smith SM, Vidaurre D, Beckmann CF, Glasser MF, Jenkinson M, Miller KL, Nichols TE, Robinson EC, Salimi-Khorshidi G, Woolrich MW, Barch DM, Uğurbil K, Van Essen DC. Functional connectomics from resting-state fMRI. Trends Cogn Sci. 2013; 17:666–682. [PubMed: 24238796]
3. Maier A, Wilke M, Aura C, Zhu C, Ye FQ, Leopold DA. Divergence of fMRI and neural signals in V1 during perceptual suppression in the awake monkey. Nat Neurosci. 2008; 11:1193–200. [PubMed: 18711393]
4. Sirotin YB, Das A. Anticipatory haemodynamic signals in sensory cortex not predicted by local neuronal activity. Nature. 2009; 457:475–9. [PubMed: 19158795]
5. Huo BX, Smith JB, Drew PJ. Neurovascular Coupling and Decoupling in the Cortex during Voluntary Locomotion. J Neurosci. 2014; 34:10975–81. [PubMed: 25122897]
6. Vazquez AL, Fukuda M, Crowley JC, Kim S-G. Neural and Hemodynamic Responses Elicited by Forelimb- and Photo-stimulation in Channelrhodopsin-2 Mice: Insights into the Hemodynamic Point Spread Function. Cereb Cortex. 2014; :2908–2919. DOI: 10.1093/cercor/bht147 [PubMed: 23761666]
7. Drew PJ, Shih AY, Kleinfeld D. Fluctuating and sensory-induced vasodynamics in rodent cortex extend arteriole capacity. Proc Natl Acad Sci U S A. 2011; 108:8473–8. [PubMed: 21536897]
8. Gao YR, Ma Y, Zhang Q, Winder AT, Liang Z, Antinori L, Drew PJ, Zhang N. Time to wake up: Studying neurovascular coupling and brain-wide circuit function in the un-anesthetized animal. Neuroimage. 2017; 153:382–398. [PubMed: 27908788]
9. Huo BX, Gao YR, Drew PJ. Quantitative separation of arterial and venous cerebral blood volume increases during voluntary locomotion. Neuroimage. 2015; 105:369–379. [PubMed: 25467301]
10. Hall CN, Reynell C, Gesslein B, Hamilton NB, Mishra A, Sutherland Ba, O'Farrell FM, Buchan AM, Lauritzen M, Attwell D. Capillary pericytes regulate cerebral blood flow in health and disease. Nature. 2014; 508:55–60. [PubMed: 24670647]
11. Kim SG, Ogawa S. Biophysical and physiological origins of blood oxygenation level-dependent fMRI signals. J Cereb Blood Flow Metab. 2012; 32:1188–1206. [PubMed: 22395207]
12. Logothetis NK. What we can do and what we cannot do with fMRI. Nature. 2008; 453:869–78. [PubMed: 18548064]
13. Hirano Y, Stefanovic B, Silva AC. Spatiotemporal Evolution of the fMRI Response to Ultrashort Stimuli. J Neurosci. 2011; 31:1440–1447. [PubMed: 21273428]
14. Fukuda M, Rajagopalan UM, Homma R, Matsumoto M, Nishizaki M, Tanifuji M. Localization of activity-dependent changes in blood volume to submillimeter-scale functional domains in cat visual cortex. Cereb Cortex. 2005; 15:823–833. [PubMed: 15459078]
15. Guipponi O, Odouard S, Pinede S, Wardak C, Ben Hamed S. fMRI Cortical Correlates of Spontaneous Eye Blinks in the Nonhuman Primate. Cereb Cortex. 2014; 25:2333–2345. [PubMed: 24654257]
16. Galton F. The Measure of Fidget. Nature. Jun.1885 :174–175.
17. O'Connor DH, Hires SA, Guo ZV, Li N, Yu J, Sun QQ, Huber D, Svoboda K. Neural coding during active somatosensation revealed using illusory touch. Nat Neurosci. 2013; 16:958–965. [PubMed: 23727820]
18. Liu X, Duyn JH. Time-varying functional network information extracted from brief instances of spontaneous brain activity. Proc Natl Acad Sci U S A. 2013; 110:4392–7. [PubMed: 23440216]
19. Laumann TO, Snyder AZ, Mitra A, Gordon EM, Gratton C, Adeyemo B, Gilmore AW, Nelson SM, Berg JJ, Greene DJ, McCarthy JE, Tagliazucchi E, Laufs H, Schlaggar BL, Dosenbach NUF, Petersen SE. On the Stability of BOLD fMRI Correlations. Cereb Cortex. 2016; :1–14. DOI: 10.1093/cercor/bhw265 [PubMed: 25139941]
20. Schölvinck ML, Maier A, Ye FQ, Duyn JH, Leopold DA. Neural basis of global resting-state fMRI activity. Proc Natl Acad Sci U S A. 2010; 107:10238–43. [PubMed: 20439733]

21. Theis L, Berens P, Froudarakis E, Reimer J, Román Rosón M, Baden T, Euler T, Tolias AS, Bethge M. Benchmarking Spike Rate Inference in Population Calcium Imaging. Neuron. 2016; 90:471–482. [PubMed: 27151639]
22. Goense JBM, Logothetis NK. Neurophysiology of the BOLD fMRI signal in awake monkeys. Curr Biol. 2008; 18:631–40. [PubMed: 18439825]
23. de Kock CPJ, Sakmann B. Spiking in primary somatosensory cortex during natural whisking in awake head-restrained rats is cell-type specific. Proc Natl Acad Sci U S A. 2009; 106:16446–50. [PubMed: 19805318]
24. Chapin JK, Lin CS. Mapping the body representation in the SI cortex of anesthetized and awake rats. J Comp Neurol. 1984; 229:199–213. [PubMed: 6438190]
25. Sachidhanandam S, Sreenivasan V, Kyriakatos A, Kremer Y, Petersen CCH. Membrane potential correlates of sensory perception in mouse barrel cortex. Nat Neurosci. 2013; 16:1671–7. [PubMed: 24097038]
26. Boynton GM, Engel Sa, Glover GH, Heeger DJ. Linear systems analysis of functional magnetic resonance imaging in human V1. J Neurosci. 1996; 16:4207–21. [PubMed: 8753882]
27. Kay KN, Naselaris T, Prenger RJ, Gallant JL. Identifying natural images from human brain activity. Nature. 2008; 452:352–355. [PubMed: 18322462]
28. O'Connor DH, Clack NG, Huber D, Komiyama T, Myers EW, Svoboda K. Vibrissa-Based Object Localization in Head-Fixed Mice. J Neurosci. 2010; 30:1947–1967. [PubMed: 20130203]
29. Sreenivasan V, Esmaeili V, Kiritani T, Galan K, Crochet S, Petersen CCH. Movement Initiation Signals in Mouse Whisker Motor Cortex. Neuron. 2016; 92:1368–1382. [PubMed: 28009277]
30. Howarth C, Gleeson P, Attwell D. Updated energy budgets for neural computation in the neocortex and cerebellum. J Cereb Blood Flow Metab. 2012; 32:1222–32. [PubMed: 22434069]
31. Logothetis NK, Pauls J, Augath M, Trinath T, Oeltermann a. Neurophysiological investigation of the basis of the fMRI signal. Nature. 2001; 412:150–7. [PubMed: 11449264]
32. Cardoso MMB, Sirotin YB, Lima B, Glushenkova E, Das A. The neuroimaging signal is a linear sum of neurally distinct stimulus- and task-related components. Nat Neurosci. 2012; 15:1298–306. [PubMed: 22842146]
33. Murphy K, Birn RM, Bandettini PA. Resting-state fMRI confounds and cleanup. Neuroimage. 2013; 80:349–359. [PubMed: 23571418]
34. Attwell D, Buchan AM, Charpak S, Lauritzen M, Macvicar Ba, Newman Ea. Glial and neuronal control of brain blood flow. Nature. 2010; 468:232–43. [PubMed: 21068832]
35. Mayhew JEW, Askew S, Zheng Y, John P, Westby GM, Redgrave P, Rector DM, Harper RM. Cerebral Vasomotion: A 0.1-Hz Oscillation in Reflected Light Imaging of Neural Activity. Neuroimage. 1996; 4:183–196. [PubMed: 9345508]
36. Thrane AS, Thrane VR, Zeppenfeld D, Lou N, Xu Q, Nagelhus Ea, Nedergaard M. General anesthesia selectively disrupts astrocyte calcium signaling in the awake mouse cortex. Proc Natl Acad Sci. 2012; 109:18974–18979. [PubMed: 23112168]
37. Osol G, Halpern W. Spontaneous vasomotion in pressurized cerebral arteries from genetically hypertensive rats. Am J Physiol. 1988; 254:H28–33. [PubMed: 3337256]
38. Wölfle SE, Chaston DJ, Goto K, Sandow SL, Edwards FR, Hill CE. Non-linear relationship between hyperpolarisation and relaxation enables long distance propagation of vasodilatation. J Physiol. 2011; 589:2607–23. [PubMed: 21486765]
39. Gao YR, Greene SE, Drew PJ. Mechanical restriction of intracortical vessel dilation by brain tissue sculpts the hemodynamic response. Neuroimage. 2015; 115:162–176. [PubMed: 25953632]
40. Mishra A, Reynolds JP, Chen Y, Gourine AV, Rusakov DA, Attwell D. Astrocytes mediate neurovascular signaling to capillary pericytes but not to arterioles. Nature. 2016; 19:1619–1630.
41. Chaigneau E, Tiret P, Lecoq J, Ducros M, Knöpfel T, Charpak S. The relationship between blood flow and neuronal activity in the rodent olfactory bulb. J Neurosci. 2007; 27:6452–6460. [PubMed: 17567806]
42. Drew PJ, Duyn JH, Golanov E, Kleinfeld D. Finding coherence in spontaneous oscillations. Nat Neurosci. 2008; 11:991–3. [PubMed: 18725901]

43. van den Brink RL, Pfeffer T, Warren CM, Murphy PR, Tona KD, van der Wee NJA, Giltay E, van Noorden MS, Rombouts SARB, Donner TH, Nieuwenhuis S. Catecholaminergic Neuromodulation Shapes Intrinsic MRI Functional Connectivity in the Human Brain. J Neurosci. 2016; 36:7865–7876. [PubMed: 27466332]
44. O'Herron P, Chhatbar PY, Levy M, Shen Z, Schramm AE, Lu Z, Kara P. Neural correlates of single-vessel haemodynamic responses in vivo. Nature. 2016; 534:378–382. [PubMed: 27281215]
45. Ma Y, Kozberg MG, Kim SH, Shaik MA, Timmerman D, Hillman EMC. Resting-state hemodynamics are spatiotemporally coupled to synchronized and symmetric neural activity in excitatory neurons. Proc Natl Acad Sci. 2016; 113:E8463–E8471. DOI: 10.1073/pnas.1525369113 [PubMed: 27974609]
46. Nimmerjahn A, Mukamel EA, Schnitzer MJ. Motor Behavior Activates Bergmann Glial Networks. Neuron. 2009; 62:400–412. [PubMed: 19447095]
47. Murphy K, Birn RM, Handwerker DA, Jones TB, Bandettini PA. The impact of global signal regression on resting state correlations: Are anti-correlated networks introduced? Neuroimage. 2009; 44:893–905. [PubMed: 18976716]
48. Cauli B, Tong XK, Rancillac A, Serluca N, Lambolez B, Rossier J, Hamel E. Cortical GABA interneurons in neurovascular coupling: relays for subcortical vasoactive pathways. J Neurosci. 2004; 24:8940–9. [PubMed: 15483113]
49. Iliff JJ, Wang M, Zeppenfeld DM, Venkataraman A, Plog BA, Liao Y, Deane R, Nedergaard M. Cerebral arterial pulsation drives paravascular CSF-interstitial fluid exchange in the murine brain. J Neurosci. 2013; 33:18190–9. [PubMed: 24227727]
50. Mohajerani MH, Chan AW, Mohsenvand M, LeDue J, Liu R, McVea Da, Boyd JD, Wang YT, Reimers M, Murphy TH. Spontaneous cortical activity alternates between motifs defined by regional axonal projections. Nat Neurosci. 2013; 16:1426–35. [PubMed: 23974708]
51. Drew PJ, Shih AY, Driscoll JD, Knutsen PM, Blinder P, Davalos D, Akassoglou K, Tsai PS, Kleinfeld D. Chronic optical access through a polished and reinforced thinned skull. Nat Methods. 2010; 7:5–11. [PubMed: 20038949]
52. Drew PJ, Feldman DE. Intrinsic signal imaging of deprivation-induced contraction of whisker representations in rat somatosensory cortex. Cereb Cortex. 2009; 19:331–48. [PubMed: 18515797]
53. Shirey MJ, Smith JB, Kudlik DE, Huo BX, Greene SE, Drew PJ. Brief anesthesia, but not voluntary locomotion, significantly alters cortical temperature. J Neurophysiol. 2015; 114:309–322. [PubMed: 25972579]
54. Gehrmann J, Hammer PE, Maguire CT, Wakimoto H, Triedman JK, Berul CI. Phenotypic screening for heart rate variability in the mouse. Am J Physiol Heart Circ Physiol. 2000; 279:H733–40. [PubMed: 10924073]
55. Huo BX, Greene SE, Drew PJ. Venous cerebral blood volume increase during voluntary locomotion reflects cardiovascular changes. Neuroimage. 2015; 118:301–312. [PubMed: 26057593]
56. O'Connor SM, Berg RW, Kleinfeld D. Coherent electrical activity between vibrissa sensory areas of cerebellum and neocortex is enhanced during free whisking. J Neurophysiol. 2002; 87:2137–48. [PubMed: 11929931]
57. Ganguly K, Kleinfeld D. Goal-directed whisking increases phase-locking between vibrissa movement and electrical activity in primary sensory cortex in rat. Proc Natl Acad Sci U S A. 2004; 101:12348–53. [PubMed: 15297618]
58. Henze DA, Borhegyi Z, Csicsvari J, Mamiya A, Harris KD, Buzsáki G, Aika Y, Ren J, Kosaka K, Kosaka T, Boss B, Turlejski K, Stanfield B, Cowan W, Brooks C, Eccles J, Buhl E, Szilagyi T, Halasy K, et al. Intracellular features predicted by extracellular recordings in the hippocampus in vivo. J Neurophysiol. 2000; 84:390–400. [PubMed: 10899213]
59. Drew PJ, Blinder P, Cauwenberghs G, Shih AY, Kleinfeld D. Rapid determination of particle velocity from space-time images using the Radon transform. J Comput Neurosci. 2010; 29:5–11. [PubMed: 19459038]
60. Gao YR, Drew PJ. Effects of Voluntary Locomotion and Calcitonin Gene-Related Peptide on the Dynamics of Single Dural Vessels in Awake Mice. J Neurosci. 2016; 36:2503–2516. [PubMed: 26911696]

61. Zhao X, Chen H, Liu X, Cang J. Orientation-selective responses in the mouse lateral geniculate nucleus. J Neurosci. 2013; 33:12751–63. [PubMed: 23904611]
62. Constantinople CM, Bruno RM. Effects and mechanisms of wakefulness on local cortical networks. Neuron. 2011; 69:1061–1068. [PubMed: 21435553]
63. Napoleone P, Erd S, Amenta F. Autoradiographic localization of the GABA A receptor agonist [3H] muscimol in rat cerebral vessels. Brain Res. 1987; 423:109–115. [PubMed: 2823981]
64. de Blas AL, Vitorica J, Friedrich P. Localization of the GABAA receptor in the rat brain with a monoclonal antibody to the 57,000 Mr peptide of the GABAA receptor/benzodiazepine receptor/Cl− channel complex. J Neurosci. 1988; 8:602–14. [PubMed: 2828565]
65. Lein E, Hawrylycz M, Ao N, Ayres M, Bensinger A, Bernard A, Boe A, Boguski M, Brockway K, Byrnes E, Chen L, Chen L, Chen T, Chin M, Chong J, Crook B, Czaplinska A, Dang C, Datta S, et al. Genome-wide atlas of gene expression in the adult mouse brain. Nature. 2007; 445:168–176. [PubMed: 17151600]
66. Anenberg E, Chan AW, Xie Y, LeDue JM, Murphy TH. Optogenetic stimulation of GABA neurons can decrease local neuronal activity while increasing cortical blood flow. J Cereb Blood Flow Metab. 2015; 35:1579–1586. [PubMed: 26082013]
67. Gao YR, Drew PJ. Determination of vessel cross-sectional area by thresholding in Radon space. J Cereb Blood Flow Metab. 2014; 34:1180–1187. [PubMed: 24736890]
68. Mitra, P., Bokil, H. Observed Brain Dynamics. Oxford University Press; 2008.
69. Hutchison RM, Womelsdorf T, Allen Ea, Bandettini Pa, Calhoun VD, Corbetta M, Della Penna S, Duyn JH, Glover GH, Gonzalez-Castillo J, Handwerker Da, Keilholz S, Kiviniemi V, Leopold Da, de Pasquale F, Sporns O, Walter M, Chang C. Dynamic functional connectivity: Promise, issues, and interpretations. Neuroimage. 2013; 80:360–378. [PubMed: 23707587]
70. Glover GH. Deconvolution of impulse response in event-related BOLD fMRI. Neuroimage. 1999; 9:416–429. [PubMed: 10191170]
71. De Zwart, Ja, Silva, AC., Van Gelderen, P., Kellman, P., Fukunaga, M., Chu, R., Koretsky, AP., Frank, Ja, Duyn, JH. Temporal dynamics of the BOLD fMRI impulse response. Neuroimage. 2005; 24:667–677. [PubMed: 15652302]
72. Pisauro MA, Benucci A, Carandini M. Local and global contributions to hemodynamic activity in mouse cortex. J Neurophysiol. 2016; 115:2931–2936. [PubMed: 26984421]
73. Aarts E, Verhage M, Veenvliet JV, Dolan CV, van der Sluis S. A solution to dependency: using multilevel analysis to accommodate nested data. Nat Neurosci. 2014; 17:491–496. [PubMed: 24671065]

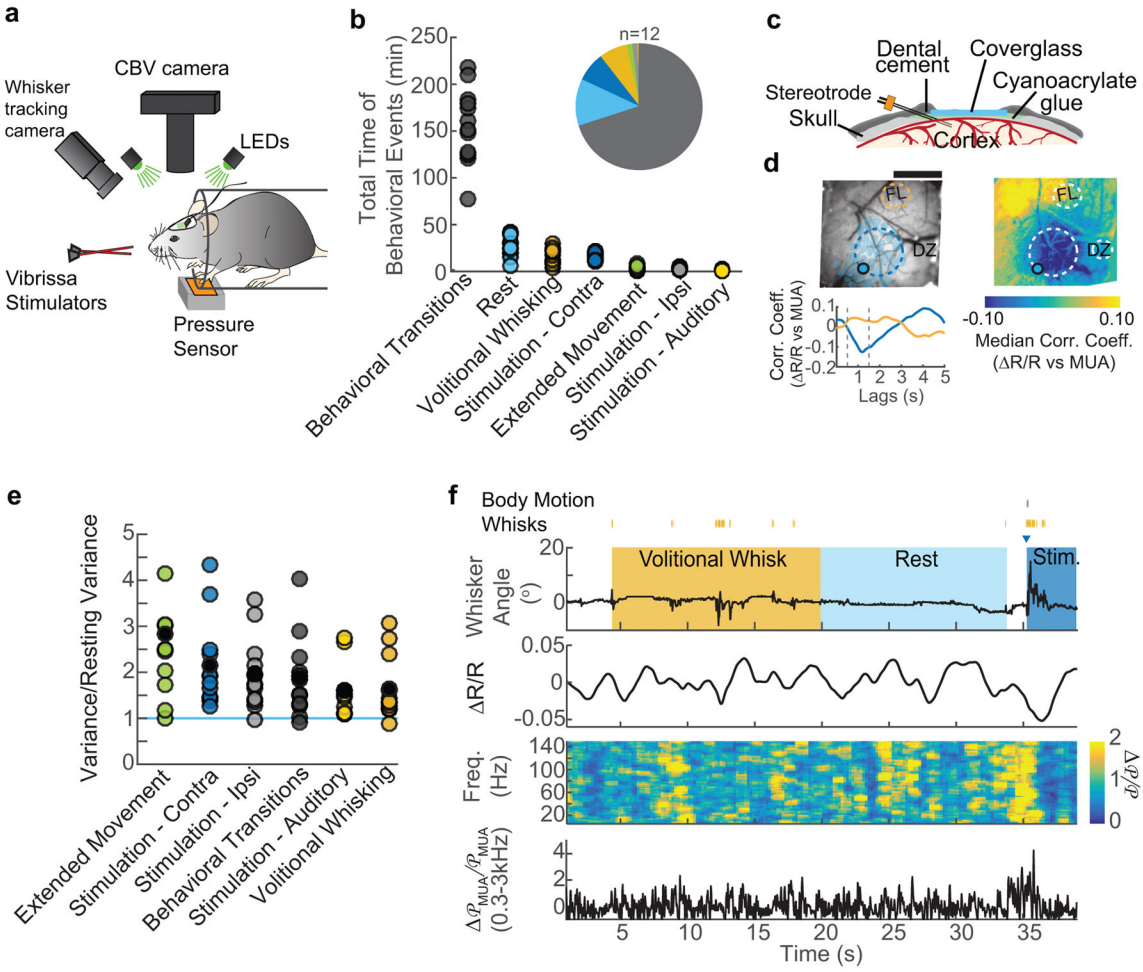

Figure 1. Behavior drives cerebral blood volume (CBV) fluctuations

a: Schematic of the experimental setup. **b:** Total behavioral times, in minutes, for each animal (circles, n=12), inset shows the median portion of recorded data corresponding to each behavior **c:** Schematic of the reinforced thinned-skull windows and implanted stereotrode. **d:** Representative example from a single animal showing that correlations between CBV (−ΔR/R) and neural activity were largest near the stereotrode for all animals (n=12). Top left: image of a thinned skull window. Filled circle indicates the reconstructed location of the stereotrode tip. Blue shaded regions show the location of whisker barrels. Dashed circular regions designate the locations of ROIs. FL, forelimb; DZ, dysgranular zone. Scale bar = 1 mm. Top right:the pixel-wise correlation coefficients between multi-unit power (300–3000 Hz) and ΔR/R during rest for the representative animal. Color denotes the median correlation coefficient for MUA lag times of 0.5–1.5 seconds (dashed vertical lines, below). Bottom left: The cross-correlation between multi-unit power and each of the anatomically-determined ROIs. Positive lags indicate that CBV follows neural activity. The dashed lines indicate the period over which the median correlation coefficient was calculated in the pixel-wise map. **e:** The variance in CBV for each state, normalized by the CBV variance during rest. Each circle represents data from single mouse (n=12). All behaviors show CBV variances significantly larger than resting variance. (Wilcoxon signed-rank,

Bonferroni corrected, extended movement: p=0.01, z=3.06 contralateral stimulation: p=0.01, z=3.06 ipsilateral stimulation: p=0.02, z=2.98; behavioral transitions: p=0.02, z=2.98; auditory stimulation: p=0.05, z=2.67; volitional whisking: p=0.02, z=2.90. **f:** Example of data from a single trial. Top: periods of volitional whisking (orange), sensory stimulation (dark blue) and rest (light blue). Vibrissae stimulation is denoted by the dark blue triangle, and volitional whisks/body movement as orange/gray tick marks, respectively. Second from top: Normalized CBV changes (ΔR/R) were measured by averaging the reflectance within the region of interest in the vibrissa cortex. Second from bottom: Normalized neural power ($\Delta P/P$) was calculated between 5–150 Hz. Bottom: MUA power was summed between 300–3000 Hz.

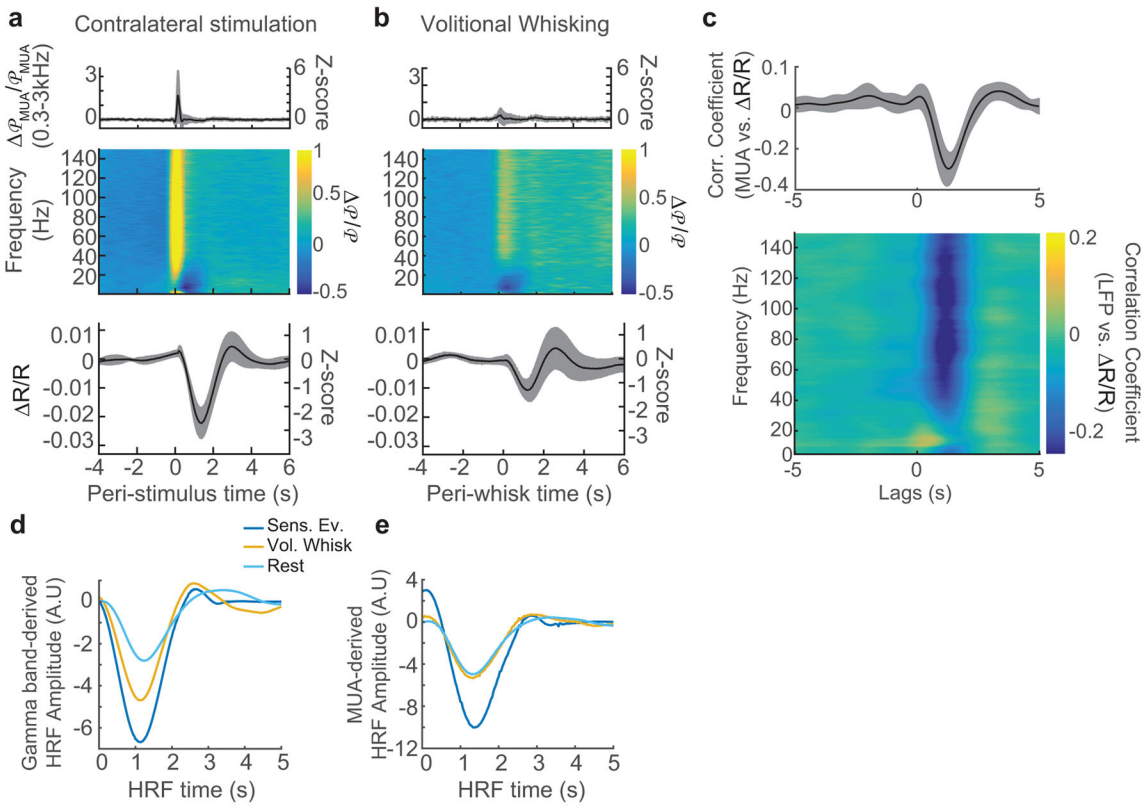

Figure 2. Neurovascular coupling was consistent across behavioral states

a: Average population (n=12 animals) responses to contralateral whisker stimulation. Top: average, normalized stimulus-evoked changes in MUA power. Middle: average, normalized stimulus-evoked changes in LFP power as a function of frequency. Bottom: reflectance change (ΔR/R) within the vibrissa ROI. **b:** Average population (n=12 animals) responses to voluntary whisker movement. Plots are organized as in **a**. Shaded areas indicate the population standard deviation. **c:** The mean cross-correlations between neural activity and ΔR/R calculated during periods of rest show that MUA power (top) and gamma-band power (bottom, 40–100 Hz) were reliably correlated with CBV changes. The shaded regions denote ±1 standard deviation (n=12 animals). CBV increases lagged neural activity changes by 1.3±0.14 seconds. **d:** A comparison of the mean gamma-band derived HRFs. Each HRF was calculated from a single behavioral state: stimulation (dark blue), volitional whisking (orange), and rest (light blue) and averaged across animals (n=12). See Figure S5 for individual data. **e:** Same as **d**, but for HRFs calculated from MUA.

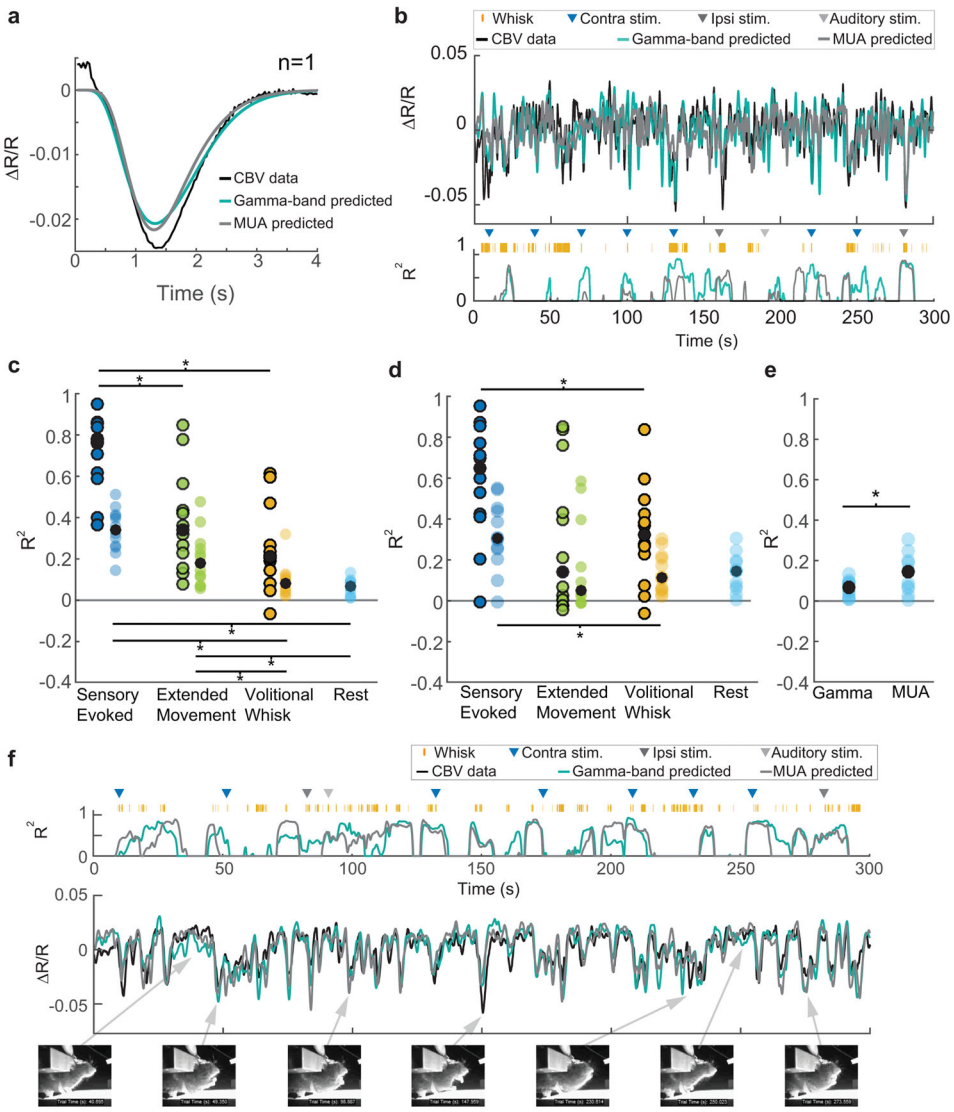

Figure 3. Predicting CBV changes from neural activity using HRFs

a: An example of the gamma-band power derived (teal blue), and MUA-derived (gray) HRFs predicting the average stimulus-triggered CBV response (black) for a single animal. Both predictions have the same dynamics as the measured response, and capture 95% of the variance (R^2=0.955; R^2=0.954). **b:** Predictions of ongoing CBV for a single trial. Top: Predictions by gamma-band (teal blue, R^2=0.29) and MUA-derived (gray, R^2=0.20 HRFs. Bottom: The goodness-of-fit (R^2) for 8-second long sliding windows. Colored triangles indicate sensory stimuli.. Orange tick marks indicate volitional whisking events. **c:** Population summary of the goodness of fit (R^2) of gamma-band power derived CBV predictions to measured CBV, separated by behavior. Circles represent the median R^2 for each animal (n=12). R^2 calculated on predictions of the average behavior-triggered CBV are outlined in black (n=12, 2-way ANOVA, $p=8\times10^{-6}$, F(2,11)=21.02. Post-hoc: Paired t-test, Bonferroni corrected, sensory evoked vs. extended movement: $p=1\times10^{-3}$, t(11)=4.36; sensory evoked vs volitional whisking: $p=6\times10^{-6}$, t(11)=8.02; extended movement vs.

volitional whisking: p=0.14, t(11)=1.57). Colored circles without black outlines indicate the median R^2 calculated for predictions of CBV during individual periods of behavior, (Friedman test, $p=3\times10^{-6}$, $\chi^2(3,33)=26.3$. Post-hoc: Wilcoxon signed rank, Bonferroni corrected. sensory evoked vs. extended movement: p=0.11, Z=2.35; sensory evoked vs. volitional whisking: p=0.02, Z=2.98, sensory evoked vs rest: p=0.01, Z=3.06, extended movement vs. volitional whisking: p=0.01, Z=3.05, volitional whisking vs. rest: p=0.51, Z=1.73, extended movement vs rest: p=0.02, Z=2.98). Filled black circles show the population medians. **d:** Same as **c**, but for MUA-derived HRFs (Averaged CBV: Friedman test, p=0.02, χ^2 (2,22)=8.17. Post-Hoc: Wilcoxon signed rank, Bonferroni corrected, sensory-evoked vs. extended movement: p=0.045, z=2.43, sensory evoked vs. volitional whisking: p=0.02, z=2.67; extended movement vs. volitional whisking: p=0.64, z=−0.47. Individual CBV: Friedman test, $p=8\times10^{-3}$, $\chi^2(3,33)=11.8$. Post-Hoc: Wilcoxon signed rank, Bonferroni corrected, sensory evoked vs. extended movement: p=0.25, z=2.04; sensory evoked vs. volitional whisk: p=0.03, z=2.82, sensory evoked vs rest: p=0.09, z=2.43; extended movement vs. volitional whisk: p=0.94, z=−0.08, extended movement vs. rest: p=0.88, z=−0.16, volitional whisk vs. rest: p=0.93, z=0.08, n=12). **e:** The MUA-derived HRF was better at predicting resting CBV fluctuations than the gamma-band power derived HRF (Paired t-test, p=0.02, t(11)=−2.68). **f:** An example illustrating that ongoing animal behavior, in this case grooming, can lead to very good prediction of measured CBV. Compare to **b** (gamma-band power derived prediction (teal blue): $R^2=0.48$, MUA-derived prediction (gray): $R^2=0.43$). Video frames showing periods of animal behavior and rest are displayed below the data. Arrows point to the data corresponding to the video frame.

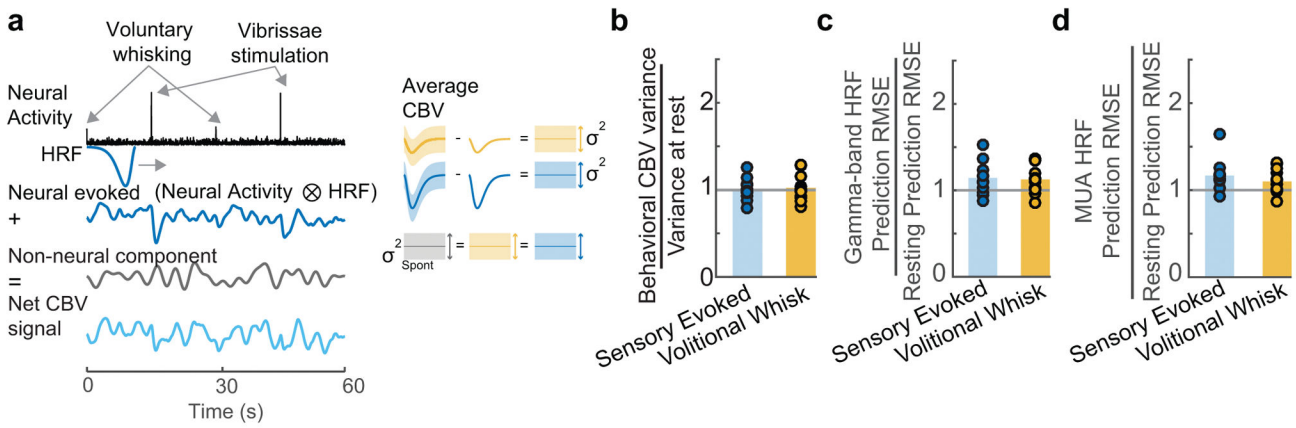

Figure 4. Variance of residual signal is similar across behavioral states

a: Schematic illustrating the hypothesis that the measured hemodynamic signal (bottom left, light blue) is comprised of a neural evoked CBV component (top left, dark blue) and a separate, additive CBV component which is uncorrelated with the measured local neural activity (middle left, gray). The neural evoked CBV component can be subtracted out using the mean response from a given behavior (top right, middle right). The variance of the residuals after subtracting the neurally-driven CBV component will be equal to the variance of the additive CBV component (bottom right). **b:** Consistent with hypothesis **a**, the variance in the mean CBV response after subtraction of the mean-evoked response was not significantly different from the variance in the CBV during rest (t-test: Sensory evoked: p=0.86, t(11)=−0.18; Whisking: p=0.61, t(11)=0.52). Each circle represents a single animal (n=12), bar indicates the mean. **c:** Comparison of the root mean squared error (RMSE) of the gamma-band derived HRF during stimulation and volitional whisking normalized by the RMSE during rest for all animals (n=12). Bars indicate the mean across animals. The RMSE was similar between behaviors for the gamma-band (t-test, Bonferroni corrected, Sensory Evoked vs. Rest: p=0.06, t(11)=2.70; Sensory Evoked vs. Whisk: 0.73, t(11)=0.35, Volitional Whisk vs. Rest: p=0.07, t(11)=2.66) **d:** Same as **c**, but for MUA derived HRF predictions (Wilcoxon signed rank, Bonferroni corrected, sensory evoked vs rest: p=0.01, z=2.90, sensory evoked vs. whisk: p=0.18, z=1.33, whisk vs. rest: p=0.07, z=2.27).

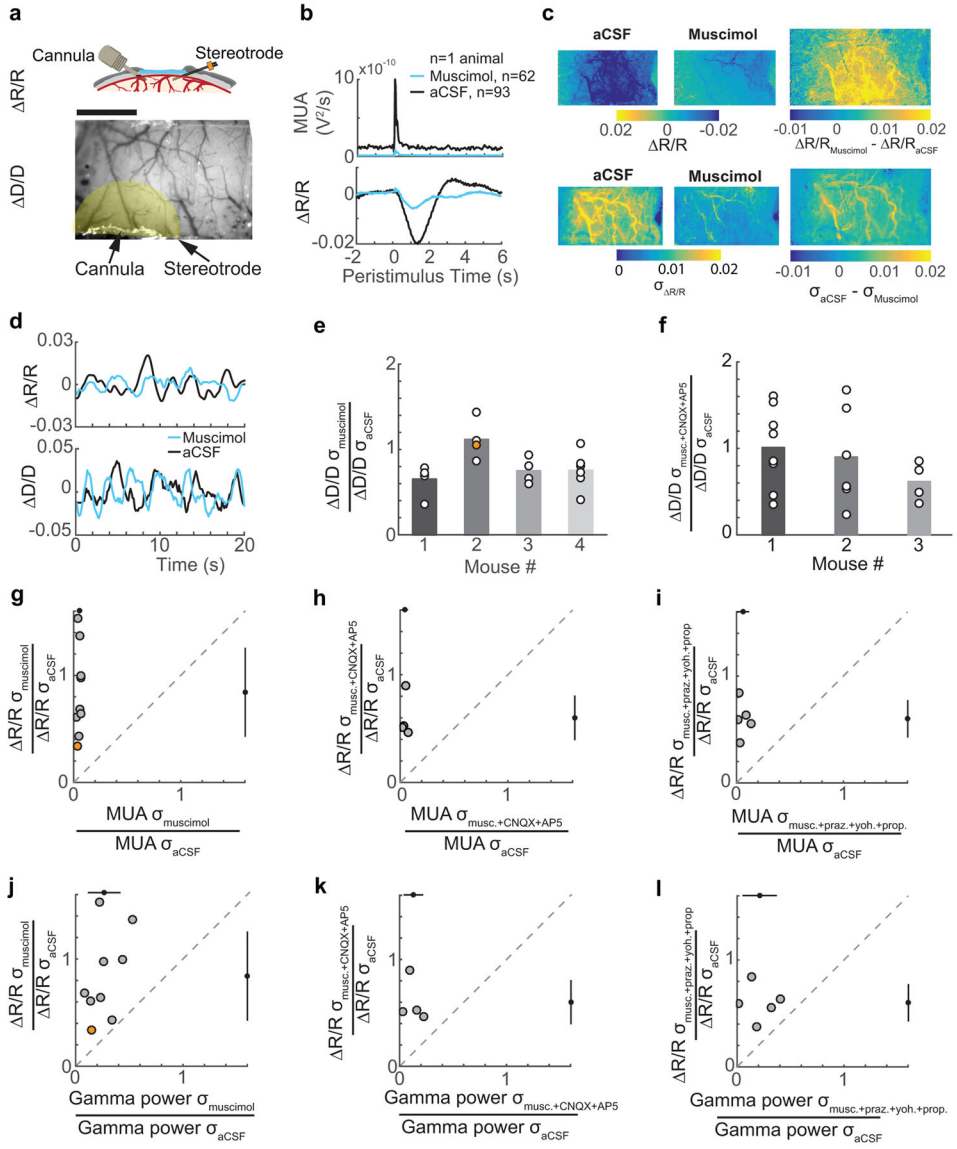

Figure 5. Spontaneous CBV fluctuations continue in the absence of neural activity and noradrenergic input

a: Top: schematic of the window-electrode-cannula preparation. Bottom: an image of a thinned-skull window with cannula and electrode implants. The shaded yellow area indicates the ROI for CBV measurements. Scale bar = 1 mm. **b:** The average stimulation-evoked MUA following muscimol (n=62 stimuli) and aCSF (n=93 stimuli) infusion in a representative animal, showing reduced baseline and sensory evoked MUA (top) and average stimulation-evoked increase in CBV (bottom) within the ROI in (**a**). **c:** The average normalized pixel-wise CBV response to contralateral whisker stimulation (0.5–2 seconds after stimulation) across the thinned skull window for a single animal after aCSF infusion (top left, n=93 stimuli) and after infusion of muscimol (top center, n=62 stimuli). Top right shows the difference between aCSF infusion and muscimol infusion in the stimulation-triggered CBV response. The root-mean squared deviation (σ) of resting CBV across the

thinned skull window after aCSF infusion (bottom left) and after muscimol infusion is shown in the bottom center. The difference in the magnitude of the fluctuations under both conditions is shown in the bottom right. Example shows the same animal depicted in **a** and **b. d:** Example of resting CBV fluctuations following aCSF (black) and muscimol (blue) infusions in a single animal (top, same animal as in **a**). Bottom, normalized diameter measurements were made from a single pial arteriole with 2-photon laser scanning microscopy following aCSF (black) and muscimol (blue) infusions from a single animal during periods of rest. **e:** Population summary of the root mean-square deviation in pial arteriole diameters (circles, n=19) after muscimol infusion for four animals. Orange circle is the arteriole in lower plot in **d**. Bars indicate the mean for each animal. Vessel diameter oscillations were reduced following infusion of muscimol compared to aCSF (Mixed-effects ANOVA, p=0.0015, t(36)=3.43) **f**: Same as **e**, except for measurements taken after infusion of muscimol+CNQX+AP5 cocktail. There was no significant difference in the amplitudes of the normalized diameter fluctuations between muscimol+CNQX+AP5 and aCSF infusions (Mixed-effects ANOVA, n=18 vessels in 3 animals, p=0.22, t(34)=1.26). **g:** A comparison of the root mean-square deviation of resting MUA and CBV fluctuations. Black circles and bars outside the axes show the populations mean and standard deviation. Orange circle is the mouse in **a–c**. The dashed gray line is the unity line. **h:** Same as **g**, except with a muscimol +CNQX+AP5 cocktail infusion. The resting CBV oscillation amplitude was not reduced compared to muscimol-only infusions (n=4, unpaired t-test, one sided, p=0.15, t(11)=1.11). **i:** Same as **g**, except with an infusion of muscimol+prazosin+yohimbine+propranolol cocktail. The resting CBV oscillation was not significantly reduced as compared to muscimol-only infusions (n=5, unpaired t-test, one-sided, p=0.12, t(12)=1.24) **j:** The root mean squared deviation of gamma-band neural power compared to CBV during periods of rest following muscimol infusion for all animals. Black circles and bars outside the axes show the populations mean and standard deviation. **k:** Same as **j**, but for infusion of muscimol+CNQX+AP5 cocktail. The resting gamma band power oscillations were reduced 87% compared to the control, but were not significantly different from reductions due to muscimol-only infusions (unpaired t-test, one-sided, p=0.06, t(11)=1.73). **l:** Same as **j**, but for an infusion of muscimol+prazosin+yohimbine+propranolol cocktail. The oscillations in gamma-band power were reduced 79% compared to aCSF control, which was not significantly different from muscimol-only infusions (unpaired t-test, two sided, p=0.52, t(12)=0.66).